Spatial Dependence of Stably Stratified Nocturnal Boundary-Layer Regimes in Complex Terrain

Carsten Abraham & Adam H. Monahan

July 2020

Boundary-Layer Meteorology (2020) 177:19–47
https://doi.org/10.1007/s10546-020-00532-x

RESEARCH ARTICLE

Spatial Dependence of Stably Stratified Nocturnal Boundary-Layer Regimes in Complex Terrain

Carsten Abraham[1] · **Adam H. Monahan**[1]

Received: 26 October 2019 / Accepted: 19 May 2020 / Published online: 23 July 2020

Abstract
The stably stratified atmospheric boundary layer (SBL) has been found in previous studies to display distinct regimes of behaviour. In particular, a contrast is often drawn between the weakly (wSBL) and very (vSBL) stable boundary layers. Time series of SBL regime affiliation obtained from hidden Markov model analyses of data from three different towers at the Los Alamos National Laboratory are used to investigate the spatial dependence of SBL regime occupation and SBL transitions. The local topography influences the flow such that south-west to north-east flow prevails, for which wSBL and vSBL conditions respectively are more likely to occur. Joint probabilities of shared regime occupation at the three towers (with and without conditioning on wind direction) are much larger than would be expected from statistically independent regime sequences at the different locations. Very persistent wSBL nights (without any transitions to the vSBL) have a higher probability of occurring across the entire tower network domain than very persistent vSBL nights. Many regime transitions occur within a narrow time window between the different towers; occurrence probabilities of such events are much higher than would be expected from statistically independent regime transitions. Of such events, transitions occurring at exactly the same time across the tower network occur most often. Many co-occurring turbulence recovery events can be associated with high-intensity intermittent turbulence events. Our results imply that the scale on which the SBL regime occupation and transitions are dependent exceeds 10 km in this region of complex terrain.

Keywords Clustering · Spatial structure · Spatial variability · Stable boundary layer · Statistics

1 Introduction

On the basis of Reynolds-averaged mean data, the stably stratified nocturnal boundary layer (SBL) is often classified into two distinct regimes denoted the weakly and very stable boundary layers (respectively, wSBL and vSBL, e.g., Mahrt 1998; Mahrt et al. 2013; Mahrt 2014;

✉ Carsten Abraham
abrahamc@uvic.ca

[1] School of Earth and Ocean Sciences, University of Victoria, P.O. Box 3065 STN CSC, Victoria, BC V8P 5C2, Canada

Mahrt et al. 2015; Acevedo and Fitzjarrald 2003; Bonin et al. 2015; van Hooijdonk et al. 2015; Monahan et al. 2015; Acevedo et al. 2016, 2019; Vignon et al. 2017; Abraham and Monahan 2019a, b, c, hereafter AM19a, AM19b, and AM19c) sometimes also denoted nearly neutral and stable regimes (Sun et al. 2012, 2016). In this classification scheme the wSBL is characterized by weak stratification, strong winds, and sustained turbulence. The vSBL, on the other hand, is characterized by strong stratification, low wind speeds, weak to collapsed turbulence, and a weak vertical coupling of the atmospheric layers. In this study we analyze the horizontal spatial structure of SBL regime occupation (which regime the SBL occupies at a particular time and place) and regime transitions across a small network of towers at the Los Alamos National Laboratory. The criteria used to distinguish SBL regimes differ between studies. Building on the results of AM19a, b, c, the present study determines regime occupation and transition statistics using the statistical technique hidden-Markov-model (HMM) analysis.

Transitions between the two SBL regimes are observed to occur frequently (AM19b). Different mechanisms drive the two types of regime transitions. Over land, the wSBL to vSBL transition (which for simplicity we denote the collapse of turbulence although weak turbulence may persist) is usually caused by radiative cooling at the surface, which strengthens the inversion and suppresses vertical turbulent fluxes of momentum and heat. This process is relatively well understood and can be explained by conceptual models (van de Wiel et al. 2007, 2017), simulations in idealized single column models (Holdsworth et al. 2016; Holdsworth and Monahan 2019), or direct numerical simulations of stratified channel flows (Donda et al. 2015; van Hooijdonk et al. 2017) or atmospheric boundary layers (Flores and Riley 2011; Ansorge and Mellado 2014). The recovery of turbulence (vSBL to wSBL transition) is more poorly understood as various mechanisms are associated with such events, including mechanical driving by increased large-scale pressure gradients or surface warming by increased cloud cover (AM19b). A more complex class of processes potentially initiating these transitions is associated with intermittent turbulence events (e.g. Mahrt 2014; Sun et al. 2015b, and references within) which have been found to dominate the turbulent transport in vSBL conditions (Nappo 1991; Coulter and Doran 2002; Doran 2004; Basu et al. 2006; Acevedo et al. 2006; Williams et al. 2013). Intermittent turbulence arises from a range of different phenomena such as breaking gravity waves or solitary waves (Mauritsen and Svensson 2007; Sun et al. 2012), density currents (Sun et al. 2002), microfronts (Mahrt 2010), Kelvin-Helmholtz instabilities interacting with the turbulent mixing (Blumen et al. 2001; Newsom and Banta 2003; Sun et al. 2012; van der Linden 2020), or shear instabilities induced from internal wave propagation (Sun et al. 2004; Zilitinkevich et al. 2008; Sun et al. 2015a). Either transition can also be caused by low-level advection of air with substantially different temperature than the atmosphere near the surface (AM19c).

While many case studies have investigated the phenomena causing regime transitions, such analyses have usually focused on transitions at individual locations in space. Relatively little research has been conducted on the spatial extent of SBL regimes and the spatial dependence of SBL regime transitions. Quantification of these structures is particularly useful for numerical weather prediction and climate models, which require representations of grid-box averages of turbulent fluxes. Parametrizations in numerical weather prediction and climate models often use long-tailed stability functions, which enhance turbulent fluxes under stable conditions to improve model performance. These functions are intended to represent unresolved subgrid-scale inhomogeneities in turbulence intensity (e.g., McCabe and Brown 2007) and potentially are a good approximation if a large-scale separation between the resolved and unresolved variables exists. For example, Medeiros and Fitzjarrald (2014) used an observational surface station network spanning a geographical area of approximately one square

degree to show that long-tailed stability functions generally provide a good representation of the heterogeneity within a model grid-box of that scale. However, Medeiros and Fitzjarrald (2014, 2015) also found that sudden turbulence increases can sometimes occur at relatively distant locations, suggesting the occurrence of intermittent turbulence events of spatial scale not much smaller than the study domain. Such a phenomenon is not accounted for by the use of long-tailed stability functions. Data from the CASES-99 field campaign (six nights) showed that intermittent turbulence events are often shared across towers 1-km apart and less often across towers 20-km apart (Coulter and Doran 2002). Some intermittent turbulent events were found by this study to extend across the entire 20-km network of towers.

Analyses of observations suggest that no clear deterministic relationship exists between regime transitions and external large-scale meteorological conditions or internal boundary-layer state variables (e.g Coulter and Doran 2002, AM19a, AM19b). For instance, while increasing (decreasing) cloud cover can be associated with times of turbulence collapse (recovery), not all cloud cover changes lead to SBL transitions, and regime transitions are in fact most often associated with no cloud cover change (AM19b). Furthermore, Coulter and Doran (2002) found that the propagation of intermittent turbulence events associated with vSBL to wSBL transitions can be upwind or downwind, without evident control by large-scale meteorological mechanisms.

Increasing computational power has lead to substantial increases in horizontal and vertical resolutions of numerical weather prediction and climate models such that the use of deterministic parametrizations employing long-tailed stability functions has become questionable. Therefore, it has been proposed that process-based explicitly stochastic parametrizations should be more appropriate to represent the SBL regime behaviour. Such parametrizations would help capture the missing transitions in the SBL and improve both climate mean states and weather forecast ensemble spread (e.g. He et al. 2012; Mahrt 2014; Nappo et al. 2014; Vercauteren and Klein 2015). A prototype of such an explicitly stochastic parametrization was developed and tested in an idealized single column model in Abraham et al. (2019, hereafter AHM19). Extending a model of SBL processes at an individual point in space to one of grid-box means requires information about the spatial coherence of regime dynamics. Furthermore, for high resolution modelling, such an analysis can further quantify how SBL regime occupation in a single grid box affects the SBL occupation of adjacent grid boxes (such as if lateral regime transition propagation should be accounted for). Finally, investigating the spatial structure of SBL regimes is not only of interest for weather and climate modelling but more generally for improving the understanding of physical processes governing the dynamics in the SBL.

In AM19a, b, c we demonstrated that the HMM analysis of Reynolds-averaged mean states can be used as a tool to systematically characterize the SBL regimes at tower sites in a range of different surface types and meteorological settings. The HMM is a statistical model that assumes that underlying a time series of observable state variables ($\mathbf{Y_t} = \{\mathbf{y_0}, \ldots, \mathbf{y_T}\}$) exists an unobserved (therefore 'hidden') discrete Markov chain ($\mathbf{X_t} = \{x_0, \ldots, x_T\}$) describing the regime dynamics of the observed system. In our analysis, the discrete Markov chain is the time series of SBL regime occupation. In each of the predefined regimes (of which we take two; cf. AM19a) the HMM associates the observations with regime-dependent parametric probability density functions (p.d.f.s). As we analyze multidimensional data, we choose the parametric p.d.f.s to be Gaussian mixture models ($P(\mathbf{y_t}|x_t = i) \sim \sum_m c_{i,m}\mathcal{N}(\mu_{i,m}, \sigma_{i,m})$, where i and m denote respectively the i-th 'hidden' regime, and m-th Gaussian mixture). As discussed in Rabiner (1989) the HMM assumptions allow determination of $P(\mathbf{Y_t}|\mathbf{\Lambda})$, where $\mathbf{\Lambda}$ denotes all HMM parameters, including the Markov chain transition matrix and regime-dependent p.d.f. parameters. Using Bayes theorem to determine $P(\mathbf{\Lambda}|\mathbf{Y_t})$ and applying a maximum-

likelihood estimation algorithm, the most likely $\mathbf{\Lambda}$ is determined, which in turn allows for the estimation of the most likely regime sequence $\mathbf{X_t}$ (c.f. Rabiner 1989; Monahan et al. 2015, AM19a). We can then use this optimal regime time series to study regime occupation and transition statistics. Unlike classical clustering techniques, the HMM estimation of $\mathbf{X_t}$ is not based just on the instantaneous state of the input variables, but takes the history of the process into account. Using vertically-averaged wind speed, vertical wind shear, and dry static stratification, we demonstrated systematically in AM19a, b, c that the HMM estimates of $\mathbf{X_t}$ produce a physically meaningful classification of observations into wSBL and vSBL regimes. A more detailed description of the HMM algorithm is presented in Rabiner (1989), and details of the HMM application to determining SBL regimes from meteorological tower data are presented in Monahan et al. (2015) and AM19a.

The analyses in AM19a, b, c only considered regime statistics at individual tower sites. As mentioned above, a next step in the development of parametrizations of regime dynamics in the SBL is the characterization of the spatial dependence of SBL regime occupation and transitions. Relatively few experimental locations exist with a network of multiple towers with sufficiently long time series to allow for obtaining a robust climatology of spatial SBL regime dependence. In this study, we focus on a network of three towers at the Los Alamos National Laboratory with a data record of about 26 years. The data are described in detail in Sect. 2, including a short discussion of the local wind statistics and the spatial dependence of SBL regime occupation and transitions is investigated in Sect. 3. Conclusions follow in Sect. 4.

2 Data

The datasets considered herein are from three different tower sites at the Los Alamos National Laboratory (TA-6, TA-49, and TA-53) containing almost 26 years of observations from February 1992 to December 2017. Excluding nights with missing data from the analysis, we use a total of 7075 nights. For these nights continuous measurements of 15-min average surface pressure; temperature 1.2 m above the surface; and wind speed, wind direction, temperature, and the horizontal (σ_u) and vertical (σ_w) components of the turbulence kinetic energy (TKE) at 11.5, 23, and 46 m are available at all stations.

The towers are located in the Pajarito Plateau in north-central New Mexico. The terrain and the position of towers are illustrated in Fig. 1. The Pajarito Plateau slopes from the west-north-west to the east-south-east with a drop of about 400 m in elevation across the whole area of the Laboratory. The intertower separations are 5.7, 6, and 7.5 km with a maximum difference in elevation of about 130 m. To the west of the tower sites lie the Jemez Mountains, which exceed the plateau elevation by approximately 900 m. The terrain is characterized by canyons and mesas that run downhill (e.g., Rishel et al. 2003; Bruggeman 2017).

All three towers are located on mesas with at least a 100-m-long fetch over short grass in the slope direction. Surface roughnesses are therefore similar across the different locations. The local downward slopes to the east of the towers are about 2, 1.7, and 1.5 degrees, for TA-6, TA-49, and TA-53 respectively. Downward slopes perpendicular to the main south-east downward slope are below 0.1 and about 0.25 degrees to the south for TA-6 and TA-49 and about 0.6 degrees to the north for TA-53. While TA-6 and TA-49 are located in the middle of their approximately 300 m wide mesas, TA-53 is located about 50 m from the edge of the adjacent canyon, which with a depth of about 70 m is also the deepest canyon in the vicinity of the three sites.

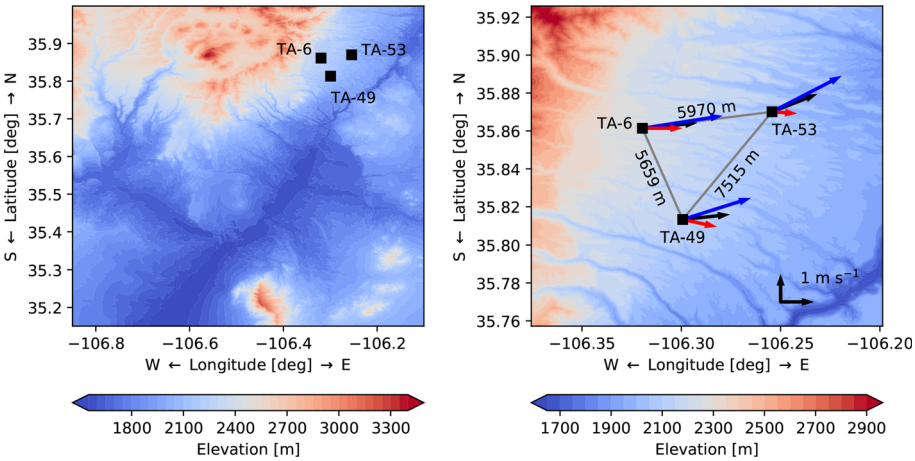

Fig. 1 Topography around the Los Alamos National Laboratory and the locations of the three towers TA-6 (35.8614 N, 106.3196 W, 2263 m), TA-49 (35.8133 N, 106.2993 W, 2147 m), and TA-53 (35.8701 N, 106.2543 W, 2130 m). In the right panel the distance between the towers is shown as well as the vector mean wind (at 46 m) at each stations for all data (black), and for wSBL (blue) and vSBL (red) conditions. The topographic data are provided by the Japan Aerospace Exploration Agency through the Advanced Land Observing Satellite (ALSO) Global Digital Surface Model

To calculate the SBL regime occupation sequence with the HMM analysis at each tower site we use a three-dimensional state variable vector consisting of vertically-averaged wind speed (between 46 and 11.5 m), wind speed shear (between 46 and 11.5 m), and potential temperature difference (between 46 and 1.2 m). All towers share these common measurement heights, which are appropriate to estimate SBL regime sequences accurately at this location (cf. AM19a). Potential temperatures are calculated from temperatures and surface pressures assuming hydrostatic equilibrium using an acceleration due to gravity of $9.81\,\mathrm{m\,s^{-2}}$, a specific heat capacity of $1005\,\mathrm{J\,kg^{-1}\,K^{-1}}$, and the specific gas constant of dry air of $287\,\mathrm{J\,kg^{-1}\,K^{-1}}$.

As described in AM19a, we define the duration of the night for the HMM analyses in terms of the surface energy budget. Net radiative loss at the surface leads to surface cooling and inversion growth (e.g, van Hooijdonk et al. 2017; Holdsworth and Monahan 2019). Consequently, we define the beginning of the night as the time when the spatially mean net radiative surface flux [Q_N; sum of upwelling and downwelling longwave (LWR) and shortwave radiation (SWR)] across tower sites becomes negative. The end of the night is defined as the time when the spatial mean Q_N becomes positive. The onset of the night defined in this way is generally earlier than sunset or the time that downwelling SWR becomes zero. While sunrise often occurs together with Q_N becoming positive, in some cases sunrise is earlier. Based on our definition, nights are found to last as long as 15 hours.

While daytime flow patterns at the different tower sites change substantially with season (via the North American monsoon), night-time flow patterns are generally characterized by downslope weak flow throughout the year, and seasonal variations are negligible (Bruggeman 2017). Nocturnal wind roses at 46 m (also including data slightly before sunset) confirm the prevailing weak downslope flow (Fig. 2, top row). While wind directions at TA-6 are broadly distributed across south to north-west winds, at TA-53 the most likely wind directions are from the south-west or north-east. TA-49 has a wind direction distribution that is intermediate between those of the other two stations, with south-westerly and north-westerly winds being the most likely but also with relatively frequent westerly winds. The time-mean night-time

wind vector is from the south-west at all sites, consistent with the prevailing downslope flow of cold air (Fig. 1, right panel). Across all stations, easterly to southerly flow is rare and only associated with low wind speeds, and as such probably reflect localized flow patterns in the absence of strong large-scale pressure gradients (Bruggeman 2017). At 46 m above the surface, wind-speeds above 8 (10) $\mathrm{m\,s^{-1}}$ occur in only 6.7 % (2.8 %), 5.8 % (2.2 %), and 6.4 % (2.1 %) of the datasets at TA-6, TA-49, and TA-53 respectively. Wind speeds below 2 $\mathrm{m\,s^{-1}}$ are much more frequent and occur in 25.3 %, 19.5 %, and 22.5 % at respectively TA-6, TA-49, and TA-53.

3 Results

In this section we first discuss the Reynolds-average mean and turbulence characteristics in the two SBL regimes at the different tower sites. We then present the regime occupation statistics and associated flow patterns at the three tower sites individually. Three statistical aspects of the spatial dependence of SBL statistics are then investigated: probabilities of shared regime occupation, of shared very persistent nights (defined as nights spent in a single regime), and of contemporaneous transitions (which we define as regime transitions that are not necessarily simultaneous but occur within a $\pm$ 2 hour time window across different towers). An assessment of the temporal dependence of regime transitions across the tower sites (that is, the timing of transitions at one site relative to that at others) follows. We then assess if meteorological state variables observed at the towers contain predictive information regarding the occurrence or absence of contemporaneous transitions. Finally, we present case studies representing different types of contemporaneous turbulence recovery events suggestive of different physical causes. All analyses below consider the complete set of nights with continuous measurements; the results are insensitive to seasonal variations.

3.1 Stably Stratified Nocturnal Boundary-Layer Characteristics

Consistent with the results of AM19a (which included TA-6), night-time scatterplots of the three-dimensional state-variable space of vertical-mean wind speed, scalar wind speed shear, and stratification exhibit a clear two-regime structure across all considered tower sites (Fig. 3). As discussed in detail in AM19a, b, c, the HMM produces physically reasonable SBL regime occupation sequences, which allow the classification of instantaneous states into wSBL conditions with relatively strong winds and weak stratification (blue) or vSBL conditions with relatively weak winds and strong stratification (red). The two resulting SBL regime populations overlap in a small region of state space of weak wind speed and weak stratification.

Whilst the two-regime structure in the state variable space depicted is qualitatively similar across the tower sites, the ranges of stratification values differ substantially. At TA-6 the stratification is considerably stronger in the vSBL than at the other sites. The terrain slopes at the different towerllocations likely cause these differences in stratification. The entire plateau generally experiences consistent downslope drainage flows of cold air during the night. The steeper slopes towards deeper parallel canyons likely lead to additional cold air drainage at TA-49 and TA-53, measurable by a more pronounced build up of cold air pools in the surrounding canyons (Bruggeman 2017). As a result, stratifications within the vSBL at TA-49 and TA-53 are weaker than at TA-6.

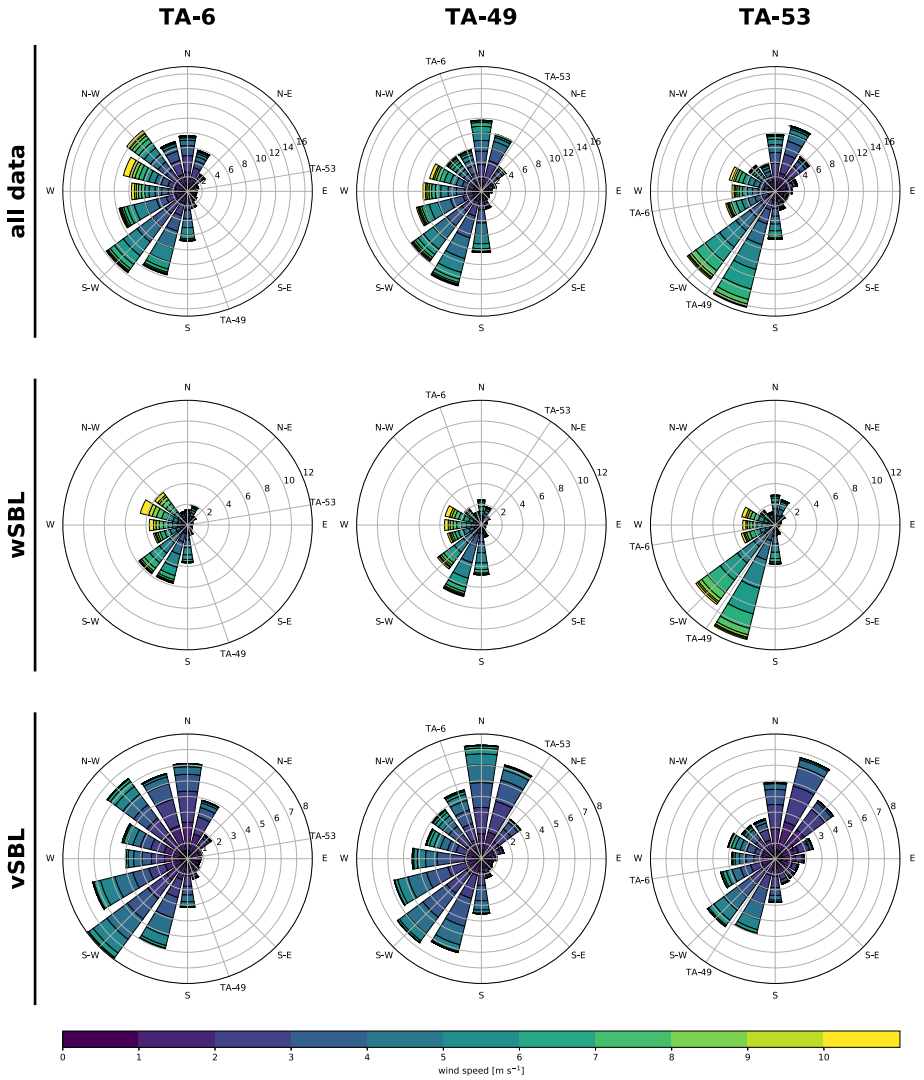

Fig. 2 Distribution of the wind directions (at 46 m, in 16 wind direction sectors) and wind speeds (at 46 m, with 11 wind speed classes denoted by colour) for all data (top row panels), and wSBL (middle row panels) and vSBL (bottom row panels) conditions at the three different tower sites (first column: TA-6; second column: TA-49; third column: TA-53). By construction, adding the distributions for the wSBL and vSBL produces the distribution of all data. The directions toward the other towers are illustrated for each site

Consistent with the inversion strengths in the two regimes, the time-mean wind vectors at 46 m at all sites have larger magnitudes in the wSBL than in the vSBL with flow from west to south-west (Fig. 1, right panel). The conditional wind direction distributions (Fig. 2) further demonstrate that the wSBL is primarily associated with moderate winds from the south-west and (less often) with stronger winds from the west. While the time-mean vSBL wind also ranges from the west to north-west at all stations (Fig. 1), vSBL conditions are associated with wind directions ranging from south-west to north-east (Fig. 2). The larger

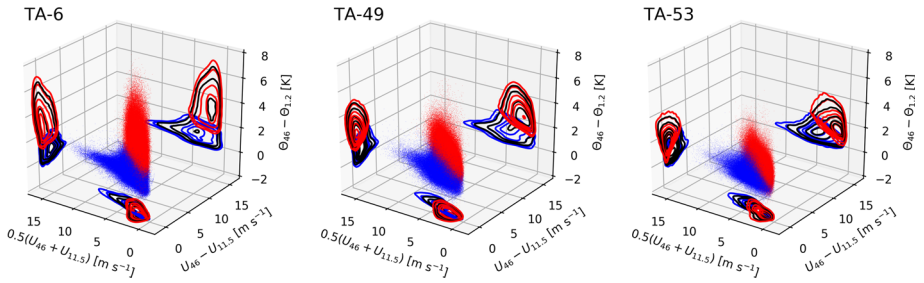

Fig. 3 Scatterplot of the three-dimensional state variable space of night-time vertical mean wind speed ($0.5(U_{46} + U_{11.5})$), scalar wind shear ($U_{46} - U_{11.5}$), and static stability ($\Theta_{46} - \Theta_{11.5}$) conditioned on HMM regimes (wSBL in blue and vSBL in red) at the three different tower sites. The bivariate joint probability distributions (calculated with the multivariate kernel density estimation of O'Brien et al. (2014, 2016)) are shown for all data (black) and wSBL (blue) and vSBL (red) conditions respectively

wind direction variability in the vSBL is likely related to the fact that vSBL conditions are usually associated with weaker pressure-gradient forces, and so wind directions are more influenced by local processes and topography than by the large-scale flow.

The p.d.f.s of wind speeds at 46 m (unconditioned on the regimes) are bimodal at TA-6 and TA-53 (Fig. 4, black). The two probability maxima correspond well with the maxima of the wind speed p.d.f.s conditioned on the two SBL regimes (Fig. 4; wSBL: blue; vSBL: red). While a bimodal p.d.f. is not found for the unconditioned wind speeds at TA-49, the conditional wind speed p.d.f.s resemble those of the other stations. The bimodality of the unconditioned wind speed p.d.f.s becomes weaker the closer the observations are to the surface such that also conditional p.d.f.s are less separated. Only at TA-53 the bimodality of the unconditioned wind-speed distribution persists at the lowest observation height. The close relationship between the peaks of the bimodal p.d.f.s and the unique maxima of the conditional p.d.f.s provides further demonstration of the effectiveness of the HMM in distinguishing the wSBL and vSBL regimes.

Across all towers, low turbulence intensities (indicated by low σ_w values) are associated with the vSBL while the long tails of the σ_w p.d.f.s are exclusively associated with wSBL conditions (Fig. 4, upper block). We choose to measure turbulence intensity by σ_w rather than TKE to avoid including energy of non-turbulent horizontal motions in the vSBL (e.g., Anfossi et al. 2005; Goulart et al. 2007; Mahrt 2011; Mortarini et al. 2016, 2019). Similar to the wind speed p.d.f.s, conditional σ_w distributions are similar across all tower stations. The large σ_w values are associated with stronger winds, which lead to larger shear production of turbulence (Fig. 4, bottom block) and weaker stratifications with less buoyant consumption. The joint p.d.f.s of wind speed and σ_w demonstrate this dependence of the turbulence intensity on the wind speed and are generally consistent with the typical hockey stick transition (HOST) pattern discussed in Sun et al. (2016).

Consistent with Sun et al. (2012, 2016) conditional wind speed p.d.f.s demonstrate a maximum wind speed above which a vSBL cannot be established (Fig. 4, black dashed lines). This wind speed threshold results from the fact that for large wind speeds turbulent sensible heat fluxes are sufficiently large to break down the stratification and establish sustained wSBL conditions (van Hooijdonk et al. 2015; van de Wiel et al. 2017). The wind-speed threshold decreases with observation height and is broadly the same across the tower network. At 46 m (11.5 m) wind speeds above 8 m s^{-1} (5 m s^{-1}) are solely associated with wSBL conditions. These relatively strong winds are associated with flow coming from the west

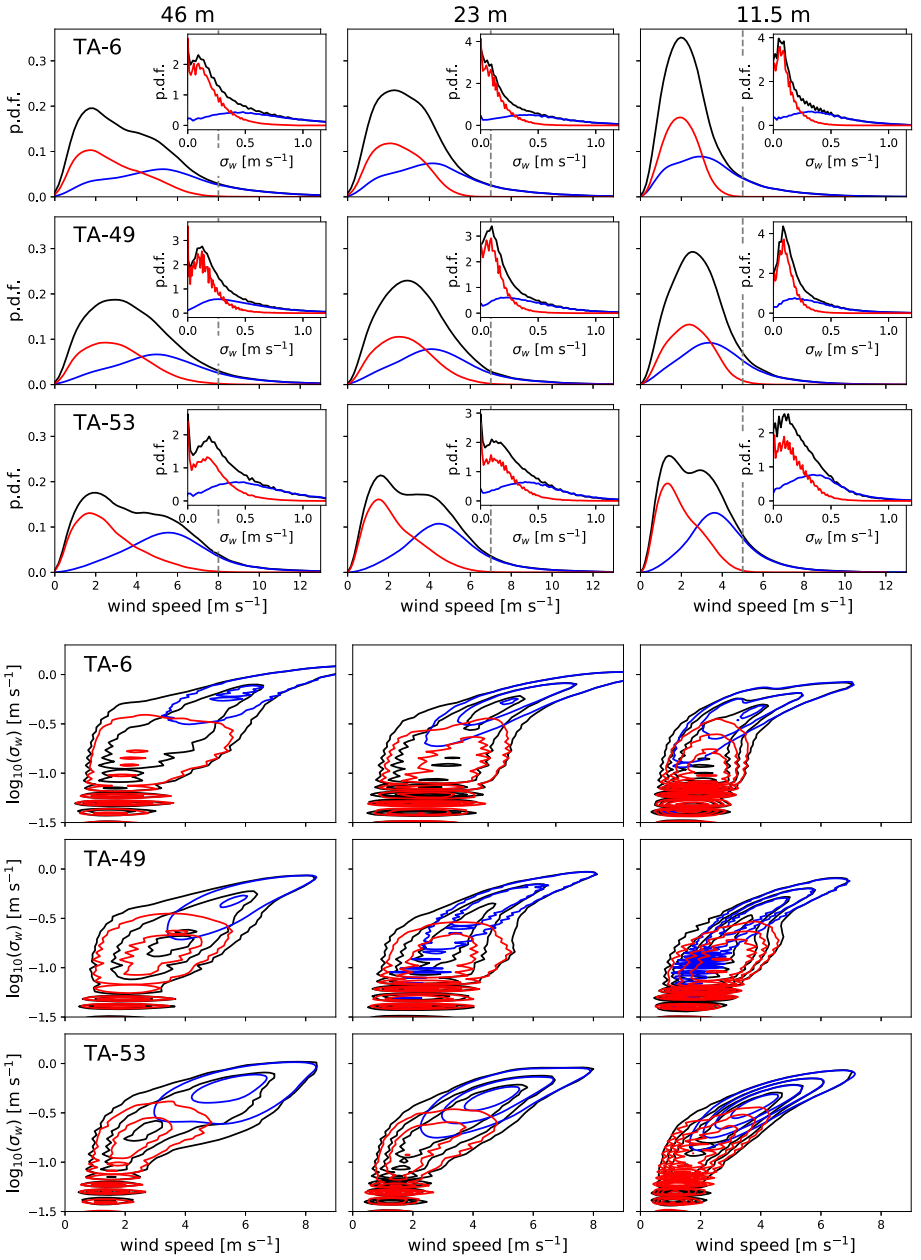

Fig. 4 Top block: Probability density functions of wind speed and σ_w (inset) measured at 46, 23, and 11.5 m for the different towers. Bottom block: Joint probability distributions of wind speeds and $\log_{10}(\sigma_w)$ for the different measurement heights and towers. All probability distributions (calculated with the multivariate kernel density estimation of O'Brien et al. (2014, 2016)) are shown for all data (black) and conditioned on wSBL (blue) and vSBL (red) conditions. The wSBL and vSBL p.d.f.s are normalized such that their sum is the p.d.f. of the full dataset

at this tower network (Fig. 2). While for specific external conditions (large-scale pressure-gradient force, low-level cloud coverage, ground heat fluxes) a specific wind-speed threshold can be determined, the long term variations of these external factors produce a continuous range of wind speed thresholds (e.g., Monahan et al. 2015; van de Wiel et al. 2017, AM19a, b, c). As a result, conditional p.d.f.s of wind speeds and σ_w overlap considerably for moderate wind speed values (although this overlap is relatively small at the highest observational level). Although we do not have information about the external conditions at Los Alamos, we find that wind variations are strongly correlated between the different towers (not shown). This fact suggests that these external conditions are relatively homogenous across the tower domain considered. Therefore, we interpret differences in SBL regime occupation between sites as being primarily a result of local processes. We now turn to the SBL regime occupation statistics at individual sites and the characteristic flow patterns in each regime.

3.2 Stably Stratified Nocturnal Boundary-Layer Regime Occupation Statistics at Individual Tower Sites

At the tower network relatively weak winds usually prevail during the night (cf. Sect. 3.1 and Bruggeman 2017). Combined with the low surface roughness at the stations the turbulence generation through wind shears is usually weak in this region. As a result turbulent sensible heat fluxes are also weak and cannot balance the night-time energy demand at the surface due to radiative cooling. Additionally, as the tower network is located in an arid environment with relatively infrequent low-level cloud coverage (Bruggeman 2017), downwelling longwave radiation is usually weak such that the night-time conditions across the network allow for effective radiative cooling of the near-surface layers and the development of stable stratifcation. Consistently, we determine higher occurrence probabilities of vSBL than wSBL conditions at all towers (cf. AM19b and Table 1). Location-specific effects result in slight variations of SBL regime statistics across the tower network. The vSBL occurs about 60 % of the time at TA-6 and TA-49 but only about 53 % of the time at TA-53 (Table 1). The higher probability of wSBL occupation at TA-53 is consistent with the relatively weak stratifications observed at this site discussed above.

About 25 % of all nights at each tower are classified as very persistent (Table 1). Again consistent with the relatively weak inversion strength at this location, TA-53 experiences a higher frequency of very persistent wSBL nights in comparison to TA-6 and TA-49. The generally stronger inversions at TA-6 are consistent with the fact that it has the highest probability of very persistent vSBL nights of all tower sites considered. Very persistent wSBL nights at each tower site occur almost exclusively for south-west winds, the direction from which winds are strongest (not shown). That very persistent wSBL nights are associated with these flow conditions is consistent with the fact that those nights require a sufficiently large and steady shear production of turbulence such that turbulent sensible heat fluxes are sufficiently large to balance the radiative cooling at the surface. In contrast, very persistent vSBL nights occur for very low wind speeds from any wind direction, with a slight preference for flow from the north to north-east (not shown).

At each tower site, at least one turbulence collapse occurs in about 70 to 75 % of all nights, whereas turbulence recovery events occur in about 40 % of all nights (Table 1). This difference is consistent with the fact that the tower network experiences night-time conditions conducive for the establishment of vSBL conditions. The likelihood of transitions occurring subsequent to a preceding turbulence collapse or recovery event is also similar at each tower site. In about 25 % of the nights that experience a turbulence collapse, multiple turbulence

Table 1 Regime statistics of the SBL at individual tower sites: regime occupation probabilities (columns 2 and 3), occurrence probabilities of at least one regime transition in a night and in brackets the occurrence probabilities of multiple regime transitions in a night conditioned that previous transitions have occurred (columns 4 and 5), and occurrence probabilities of very persistent nights (columns 6 and 7). Initial distributions of starting a night in the wSBL or vSBL are stated in columns 8 and 9

Tower	Occupation probability		Occurrence of at least one (or multiple) regime transitions		Occurrence of very persistent nights		Initial distributions	
	wSBL [%]	vSBL [%]	wSBL to vSBL [%]	vSBL to wSBL [%]	wSBL [%]	vSBL [%]	wSBL [%]	vSBL [%]
TA-6	39.65	60.35	70.02 (24.02)	37.85 (15.12)	12.44	14.39	74.52	25.48
TA-49	39.31	60.69	75.12 (23.10)	38.42 (17.00)	11.90	10.37	81.19	18.81
TA-53	46.77	53.23	69.44 (24.26)	41.81 (18.83)	16.20	10.60	77.91	22.09
at least at one tower	55.53	70.23	85.24 (40.46)	61.41 (25.18)	20.30	21.12	–	–

collapse transitions occur (Table 1). Multiple turbulence recovery events within a night occur in about 15 to 18 % of the nights that experience at least one such event. The occurrence of regime transitions at individual towers does not display a strong dependence on the wind direction (not shown). At the different towers the 46-m wind speeds during the time of regime transitions range between 2 to 7 $\mathrm{m\,s^{-1}}$ (not shown) and no clear wind speed threshold at any site is evident (cf. Fig. 4), consistent with findings in AM19a, c.

As found in AM19b, turbulence collapse events at individual towers are most likely to occur around sunset (Fig. 5, upper panel). These probability peaks of occurrence of wSBL to vSBL transitions are consistent with the fact that radiative cooling begins to occur around sunset. During such times, inversions form rapidly as surface layers cool while the air aloft remains warm from the daytime heating (van Hooijdonk et al. 2017). At TA-53 the probability maximum of wSBL to vSBL transitions shortly after sunset is weaker than at the other stations consistent with the physical properties of this site as discussed above. Beyond about two hours after sunset the probabilities of both types of transition are similar and change slowly with time. The event duration p.d.f.s in the vSBL or wSBL at each tower also show the same qualitative shape found across the suite of towers considered in AM19b (Fig. 5, lower panel). Consistent with the strong radiative cooling across the tower sites, mean event durations are slightly shorter in the wSBL than in the vSBL.

About 55 % of the time at least one tower is in the wSBL and about 70 % of the time at least one tower is in the vSBL (Table 1). Turbulence collapse occurs at at least one tower in the network in about 85 % of nights and turbulence recovery in about 60 % of the nights. All these probabilities are higher than the corresponding values at individual stations.

The general regime occupation statistics clearly reflect the overall tendency towards vSBL conditions at this tower network, consistent with the effective radiative cooling and generally low wind conditions.

Overall, the spatial regime statistics are similar across the tower network. We now investigate the dependence of regime occupation between the different sites and, in particular, the synchronization of regime transitions. As regime transitions are frequent, our analysis should include a sufficiently large number of events to obtain a robust estimate of the climatology of the spatial dependence of regime transitions.

3.3 Regime Occupation Dependence among Tower Sites

In order to assess the spatial dependence of SBL regime occupation across the network of towers, we first investigate the joint and conditional probabilities of regime occupation. With respect to developing parametrizations for SBL regime behaviour in weather and climate models these two classes of statistics yield complementary information. Joint probabilities at different locations provide information relevant to grid-box mean behaviour (assuming that all points considered are in one grid box). In the other limit, assuming that the horizontal model resolution is smaller than the dependence scale of regime occupation, conditional probabilities indicate to what extent the state of individual grid boxes will influence states of nearby grid boxes. Throughout the following analyses, we compare the observed probabilities to statistics calculated from the null hypothesis that the regime sequences at the towers are statistically independent.

The joint probability of any pair of tower sites being in the same regime varies between 79 and 87 %; the joint probability is 74.26 % for all three towers to be in the same regime (Table 2). These results clearly demonstrate spatial dependence of regime occupation. If the regime sequences were statistically independent the probabilities would be about 50 % for

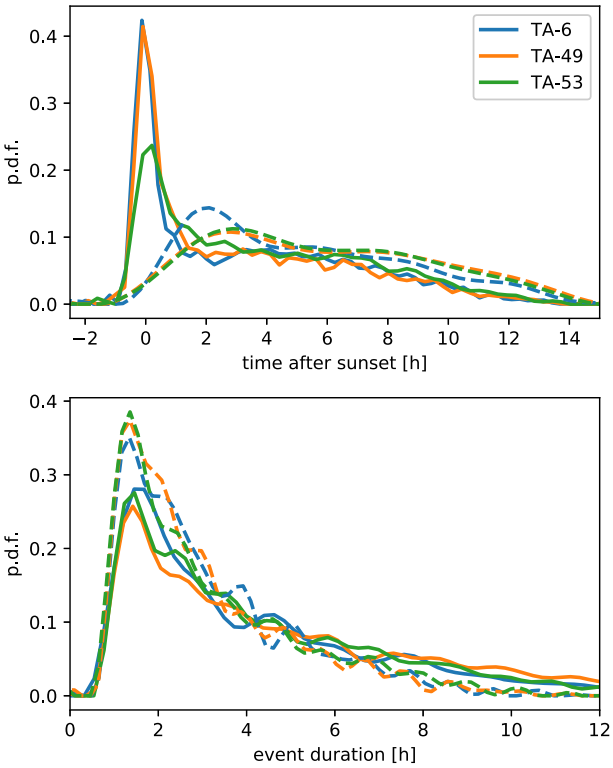

Fig. 5 Top panel: Probability density function of the timing of transitions (relative to sunset) from wSBL to vSBL (solid) and from vSBL to wSBL (dashed) at the different towers. Lower panel: Probability density function of the vSBL event duration (solid) and wSBL event duration (dashed) at the different towers. The probability density distributions are calculated with the kernel density estimation of O'Brien et al. (2014, 2016)

any pair of tower sites and 26.79 % for all three (Table 2). The joint probability of TA-6 and TA-49 being in the same regime is higher than that of either of those sites being in the same regime as TA-53. Conditional probabilities of wSBL or vSBL regimes at one tower given their occurrence at another vary between 70 to 90 %. Conditioned on the regime occupation at TA-53 a substantial difference in the conditional probabilities of the wSBL and vSBL at the other towers is observed. If TA-53 is in the wSBL, one of the other towers shares this regime about 70 % of the time. The conditional probability of a shared regime increases to about 90 % for TA-53 in the vSBL. These results demonstrate that conditions favouring the wSBL at TA-53 have weaker influence on the other sites than conditions favouring the vSBL. Similar to the joint probabilities, the conditional probabilities at all tower sites are much larger than the null hypothesis values obtained assuming statistical independence. The generally better agreement of regime occupation between TA-6 and TA-49 than with either of those sites and TA-53 is consistent with the fact that vSBL conditions are easier to break down at TA-53 than at the other sites due to its generally weaker stratifications.

When all towers are in the same regime, the flow at 46 m shows little spatial variability as wind components are relatively well correlated (Fig. 6, block 1). Naturally, wind speeds in shared wSBL conditions are larger than in shared vSBL conditions. However, even when

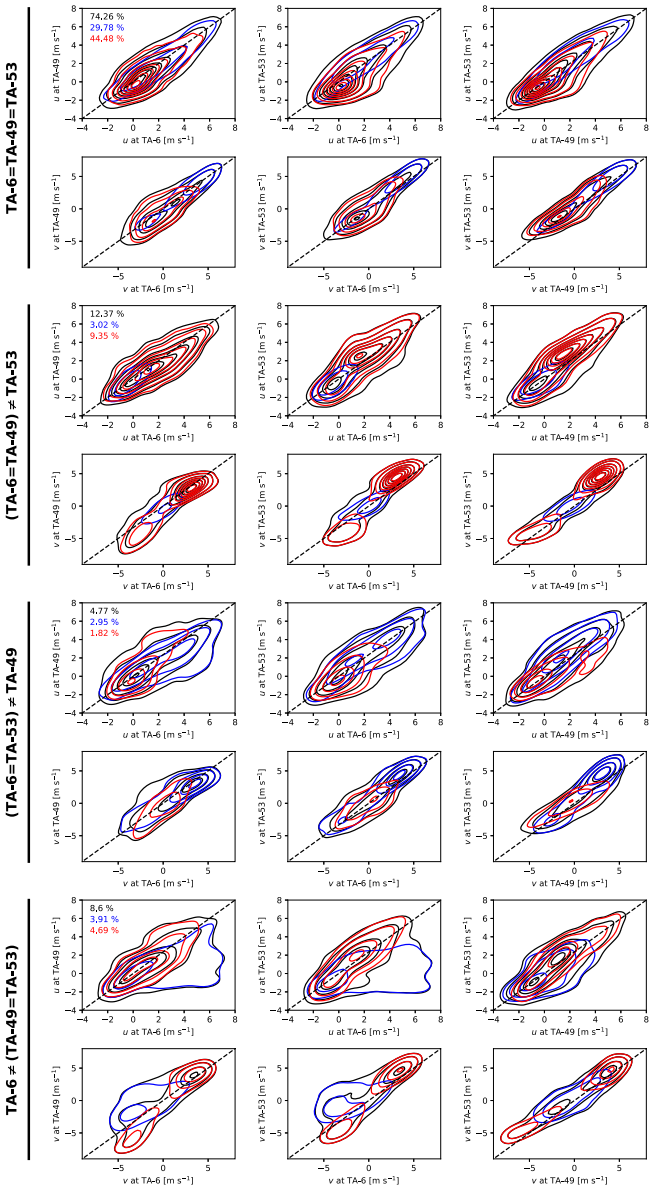

Fig. 6 Joint probability distributions of zonal wind components (u, upper panels in each block) and meridional wind components (v, lower panels in each block) at 46 m between the different tower sites, conditioned on shared SBL regime occupation; Block 1: all towers in the same regime; Block 2: TA-6 and TA-49 in the same regime; Block 3: TA-6 and TA-53 in the same regime; Block 4: TA-49 and TA-53 in the same regime. All bivariate probability distributions (calculated with the multivariate kernel density estimation of O'Brien et al. (2014, 2016)) are shown for all data (black), and the wSBL (blue) and vSBL (red) conditions at TA-6. The wSBL and vSBL joint probability distributions are normalized such that their sum is the joint probability distribution of the full dataset. Relative occurrence probabilities of the different regime occupation dependencies are stated

Table 2 Joint probabilities of shared regime occupation statistics between the tower sites (column 1). Second and third columns show the conditional probabilities of shared regime occupation across the tower sites conditioned on the tower site and the wSBL and vSBL regime. Values corresponding to statistical independence of regime sequences at the different towers are listed in brackets

	Joint probability of all data [%]	Conditional wSBL probability [%]	Conditional vSBL probability [%]
Tower	TA-6		
TA-49	86.62 (52.22)	82.69 (39.31)	89.20 (60.69)
TA-53	79.03 (50.67)	82.53 (46.77)	76.73 (53.23)
all towers	74.26 (26.79)	75.08 (18.39)	73.71 (32.31)
Tower	TA-49		
TA-6	86.62 (52.22)	83.42 (39.65)	88.69 (60.35)
TA-53	82.86 (50.70)	87.69 (46.77)	79.73 (53.23)
all towers	74.26 (26.79)	75.75 (18.54)	73.29 (32.12)
Tower	TA-53		
TA-6	79.03 (50.67)	69.97 (39.65)	86.99 (60.35)
TA-49	82.86 (50.70)	73.69 (39.31)	90.91 (60.69)
all towers	74.26 (26.79)	63.66 (15.59)	83.56 (36.63)

different tower sites are not all in the same regime, the spatial variability of the wind speed remains weak (Fig. 6, blocks 2–4). Evidently, certain strong north-west wind conditions at TA-6 are not shared by the other towers; under such conditions TA-6 is in the wSBL while TA-49 and TA-53 are in the vSBL. These strong spatial correlations of the flow are similar at other measurement heights (not shown).

The high degree of spatial correlation of the night-time flow across the tower domain was also found by Bruggeman (2017). We use the relatively large correlation to justify the interpretation that external drivers do not differ substantially across the tower domain. Therefore, in the following we consider the mean velocity at 46 m across the three towers to investigate the spatial dependence of regime occupation. We denote the magnitude of this average as $\|U\|$ and the direction from which it comes as θ.

We first investigate the joint probabilities that all three towers are or are not in the same regime conditioned on 16 different θ-sectors. In Figs. 7 and 8 these conditional joint probabilities are indicated by the length of the segments in each θ-sector. In each θ-sector we also show the relative occurrence probabilities of $\|U\|$. Probabilities corresponding to the null hypothesis of independence of the tower locations are indicated by solid red lines. The probability that all towers are in the same regime conditioned for a given θ is denoted $P(\text{all in same}|\theta)$. The complementary conditional joint probabilities that not all towers are in the same state are denoted $P(\overline{\text{all in same}}|\theta)$. The conditional joint probabilities of shared regime occupation and of $\|U\|$ falling in a particular $\|U\|$-class are denoted $P(\|U\|,\text{all in same}|\theta)$; the meaning of $P(\|U\|, \overline{\text{all in same}}|\theta)$ follows.

The probability $P(\text{all in same}|\theta)$ depends only weakly on θ and is much larger than in case if the regime occupation at the different sites was statistically independent (Fig. 7; top left panel). The lowest $P(\text{all in same}|\theta)$ values of about 70 % are found for south-westerly to south-south-westerly winds. This is the same θ range for which the pairwise probabilities $P(\text{TA-6 and TA-49 in same}|\theta)$ and $P(\text{TA-6 and TA-53 in same}|\theta)$ are the lowest (respectively about 78 % and 75 %; not shown). For all other pairs of towers and θ sectors, joint probabilities for both towers being in the same regime are between 81 % and 85 %. For south-westerly to

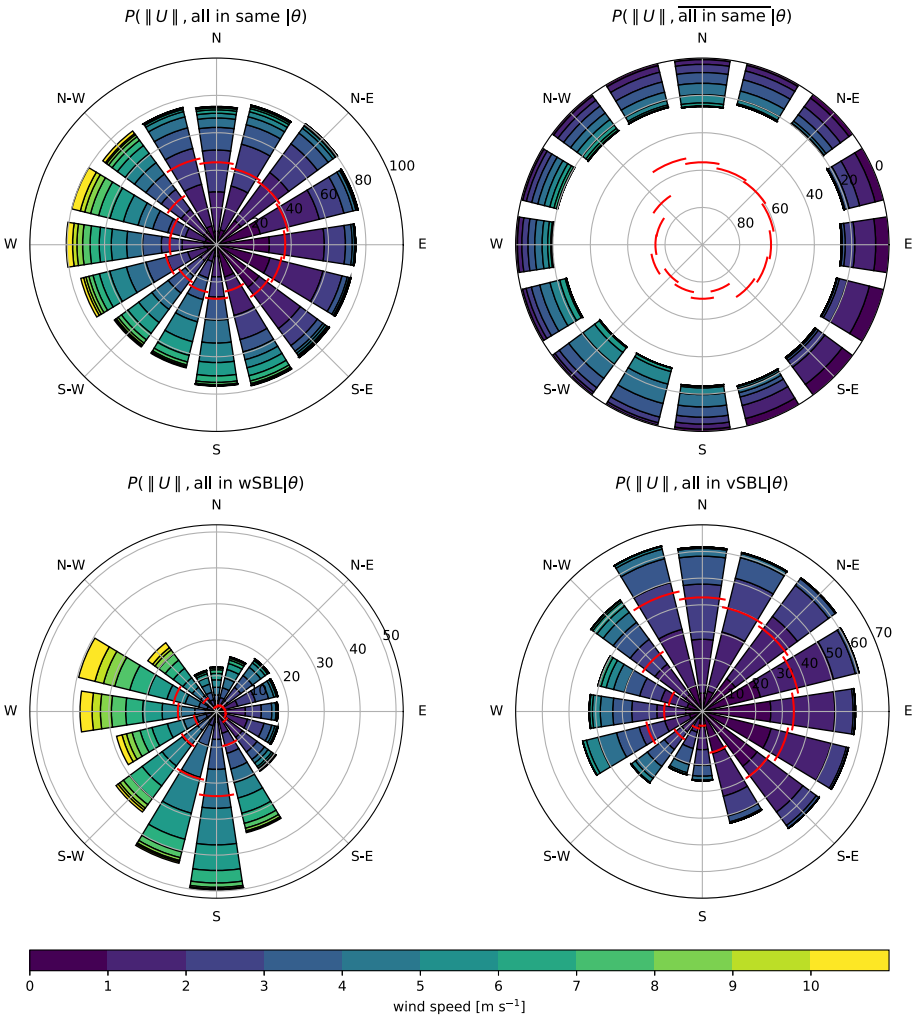

Fig. 7 Top left panel: Joint probabilities of the same regime occupation across all three tower sites and $\|U\|$ conditioned on 16 θ-sectors ($P(\|U\|, \text{all in same}|\theta)$). Within each θ-sector the distribution of $\|U\|$ is classified into 11 wind speeds (colour code), and the marginals $P(\text{all in same}|\theta)$ are indicated by the outer edges of the bars. The complimentary probabilities [not all tower sites in the same state; $P(\|U\|, \overline{\text{all in same}}|\theta)$] are depicted on the top right. Lower panels illustrate the joint probabilities of $\|U\|$ and all towers experiencing specifically wSBL [$P(\|U\|, \text{all in wSBL}|\theta)$; lower left panel] and vSBL conditions [$P(\|U\|, \text{all in vSBL}|\theta)$; lower right panel]. By construction, combining the lower panels produces the distribution in the top left panel. Red lines represent the marginal probabilities expected for statistically independent regime sequences

south-south-westerly winds TA-6 is in the lee of the Jemez Mountains whereas TA-49 and TA-53 are almost perfectly aligned along θ; the lowest joint probabilities between two and three towers for flow from this direction may result from shared regime occupation relying on unobstructed flow.

Shared regime occupation is associated with all $\|U\|$ classes. The $\|U\|$-class distribution is similar for θ sectors from the south-south-east to north-west. The $\|U\|$-class distributions in the other θ sectors are also similar to each other. The distributions $P(\|U\|, \overline{\text{all in same}}|\theta)$

(Fig. 7, upper right panel), on the other hand, show similar $\|U\|$ distributions for all θ sectors. Non-zero values of $P(\|U\|, \overline{\text{all in same}}|\theta)$ only occur for wind speeds below 7 m s^{-1}. We interpret times of relatively small $\|U\|$ as corresponding to periods of relatively weak large-scale pressure gradients, during which transitions between regimes are dominated by local processes. These conditions allow the SBL regime occupation to differ between towers. The approximate 7 m s^{-1} threshold of $\|U\|$ at 46 m indicated here falls between the 10-m and 100-m wind speeds, beyond which wSBL conditions dominate at various locations around the world (AM19a).

The probabilities conditioned on θ that all towers are in specifically the wSBL or the vSBL [$P(\text{all in wSBL}|\theta)$ and $P(\text{all in vSBL}|\theta)$, respectively] exhibit more directional dependence (Fig. 7, lower panels). The $P(\text{all in wSBL}|\theta)$ values are about 3 to 5 times larger than would be expected from statistically independent regime sequences for flows from the south to north-west. These directions are associated with stronger average flows (Fig. 2). For other wind directions values of $P(\text{all in wSBL}|\theta)$ are relatively low (below 20 %) but still about an order of magnitude higher than would be expected from statistically independent regime sequences. The $P(\text{all in vSBL}|\theta)$ values for north-west to south-east sectors are larger than those for other θ, particularly for south to south-westerly winds. All $P(\text{all in vSBL}|\theta)$ values are substantially larger than those found assuming statistical independence.

The $P(\|U\|, \text{all in vSBL}|\theta)$ values demonstrate that physical conditions that encourage shared vSBL conditions across the tower network are only associated with relatively weak flows ($\|U\|$ below 6 m s^{-1}). In contrast, nonzero $P(\|U\|, \text{all in wSBL}|\theta)$ values can be found for any $\|U\|$ class. When flows come from the south-west to north-west, the lowest $\|U\|$ associated with nonzero $P(\|U\|, \text{all in wSBL}|\theta)$ is about 3 m s^{-1}. For other θ sectors, shared wSBL conditions can occur for $\|U\|$ as low as 1 m s^{-1}. Based on the facts that $P(\|U\| > 6\,\text{m s}^{-1}, \text{all in vSBL}|\theta)$ and $P(\|U\| > 7\,\text{m s}^{-1}, \overline{\text{all in same}}|\theta)$ are zero, we conclude that $\|U\|$ above 7 m s^{-1} only occurs with the occurrence of shared wSBL conditions across the whole tower domain. Thus, with this tower domain, a $\|U\|$ threshold exists below which all combinations of regime occupation across the tower domain are possible, but above which only common wSBL conditions almost certainly prevail.

The conditional probabilities that all three towers share a common wSBL given both θ and that at least one tower is in the wSBL, $P(\text{all in wSBL}|\text{one in wSBL}, \theta)$, shows less θ-dependence than the conditional joint probabilities discussed before (Fig. 8). The same is true for $P(\text{all in vSBL}|\text{one in vSBL}, \theta)$. The values of $P(\text{all in wSBL}|\text{one in wSBL}, \theta)$ are about 60 % for south- to north-easterly winds and about 49 % for the other wind sectors (all about an order of magnitude larger than the values expected from statistically independent regime sequences). Values of $P(\text{all in vSBL}|\text{one in vSBL}, \theta)$ are about 75 % for most wind directions. The relatively small values of $P(\text{all in vSBL}|\text{one in vSBL}, \theta)$ for south to south-westerly flows may be due to the fact that the TA-6 tower is in the lee of the Jemez Mountains and may experience relatively weak winds conducive to a vSBL regime at the same time TA-49 and TA-53 experience stronger winds.

The joint probability of shared very persistent wSBL nights at all towers is about 8 %, twice as high as that for very persistent vSBL nights (Table 3, upper block). These probabilities are only slightly higher for joint probabilities of very persistent nights at pairs of tower sites. That is, if very persistent nights occur at any two stations, they typically occur at all three. The joint probabilities of shared very persistent nights are about five times higher than would be expected for statistically independent occurrences for pairs of towers and an order of magnitude higher for all three towers. The joint probability of shared very persistent wSBL nights is likely higher than that of shared very persistent vSBL nights due to the spatial localization of some turbulence events driving vSBL to wSBL transitions at individual

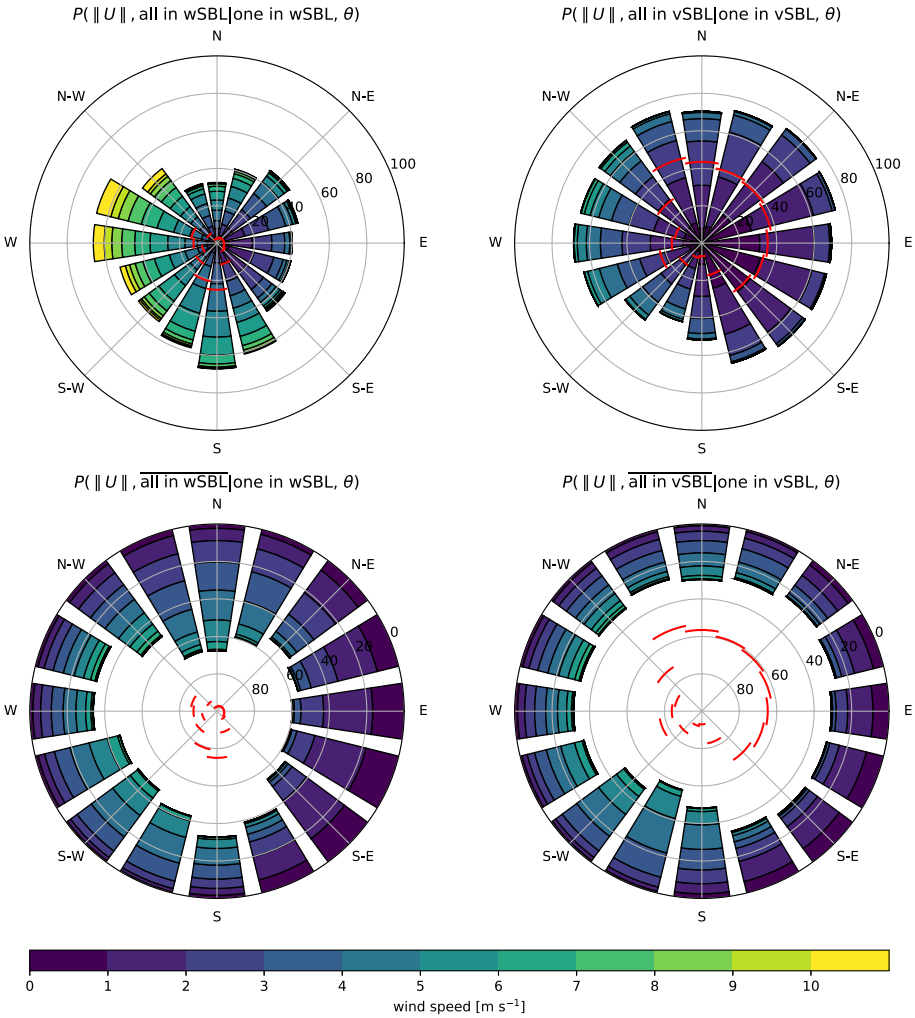

Fig. 8 Top row: Conditional joint probabilities of shared wSBL or vSBL conditions conditioned on 16 θ sectors and the fact that respectively at least one tower experiences wSBL [$P(\|U\|$, all in wSBL|one in wSBL, $\theta)$; top left panel] or vSBL conditions [$P(\|U\|$, all in vSBL|one in vSBL, $\theta)$; top right panel]. Within each θ sector the distribution of $\|U\|$ is classified into 11 wind speeds (colour code), so that the marginals P(all in wSBL| one in wSBL, θ) and P(all in vSBL| one in vSBL, θ) are equal to the outer edges of the bars. Complimentary distributions (not all tower sites in a single regime; $P(U, \overline{\text{all in wSBL}}|\text{one in wSBL}, \theta)$ and $P(\|U\|, \overline{\text{all in vSBL}}|\text{one in the vSBL}, \theta)$) are illustrated in the bottom row panels. Red lines represent the marginal probabilities expected for statistically independent regime sequences for the 16 θ sectors

sites. Very persistent wSBL nights, on the other hand, are generally associated with strong winds consistent with synoptic-scale features. We find shared very persistent wSBL nights exclusively for flows with $\|U\| > 7\,\mathrm{m\,s^{-1}}$ and coming from the south-south-west to west (not shown). Shared very persistent vSBL conditions have a much weaker spatial dependence and only occur with $\|U\| < 3\,\mathrm{m\,s^{-1}}$ (not shown).

The probability of shared very persistent wSBL nights at pairs of towers conditioned on such a night occurring at a given station is highest conditioning on TA-6 or TA-49 (Table 3,

Table 3 Joint probabilities of shared very persistent nights across the different tower sites (upper block) and conditional probabilities of the shared occurrence of very persistent nights conditioned on the regime sequence at each site (towers in the first row of the lower block). Values corresponding to statistical independence of regime occupation sequences at the different towers are listed in brackets

Tower	TA-6		TA-49		TA-53	
	wSBL [%]	vSBL [%]	wSBL [%]	vSBL [%]	wSBL [%]	vSBL [%]
Joint probabilities						
TA-6	–	–	9.34	7.40	9.28	5.78
	–	–	(1.48)	(1.49)	(2.02)	(1.53)
TA-49	9.34	7.40	–	–	9.65	5.48
	(1.48)	(1.49)	–	–	(1.93)	(1.10)
TA-53	9.28	5.78	9.65	5.48	–	–
	(2.02)	(1.53)	(1.93)	(1.10)	–	–
all towers	8.03	4.42	8.03	4.42	8.03	4.42
	(0.24)	(0.16)	(0.24)	(0.16)	(0.24)	(0.16)
Conditional probabilities						
TA-6	–	–	78.50	71.39	57.28	54.53
	–	–	(12.44)	(14.39)	(12.44)	(14.49)
TA-49	75.11	51.47	–	–	59.57	51.73
	(11.90)	(10.37)	–	–	(11.90)	(10.37)
TA-53	74.54	40.18	81.12	52.86	–	–
	(16.20)	(10.60)	(16.20)	(10.60)	–	–
all towers	64.55	30.75	67.46	42.64	49.57	41.70
	(1.92)	(1.10)	(2.02)	(1.53)	(1.48)	(1.49)

lower block). Very persistent wSBL nights at these towers are accompanied about 75 to 80 % of the time by these persistent conditions elsewhere. Conditional probabilities of shared very persistent vSBL nights are about 50 % for all tower pairs (with the exception of TA-49 conditioned on TA-6).

3.4 Regime Transition Dependence among Tower Sites

Having considered the spatial dependence of regime occupation, we now investigate the spatial dependence of regime transitions. As a first metric we define *contemporaneous* transitions as those occurring within a $\pm$ 2 h time window centred at a reference transition. This time window is sufficiently wide to contain advective time scales between towers for wind speeds as low as 1 m s^{-1}. Time scales of phenomena such as density currents or gravity waves (which could result in systematic propagation of vSBL to wSBL transitions through the tower domain) should also be within this time window. We further describe as *simultaneous* those transitions at different towers occurring at exactly the same time (within the resolution of the 15-min mean data).

In order to compare the statistics of contemporaneous and simultaneous regime transition probabilities to those expected from statistically independent regime sequences, we simulate an ensemble of 100 25-year synthetic regime sequences of individual nights (comparable to the observation record length) by sampling randomly from the climatological distributions

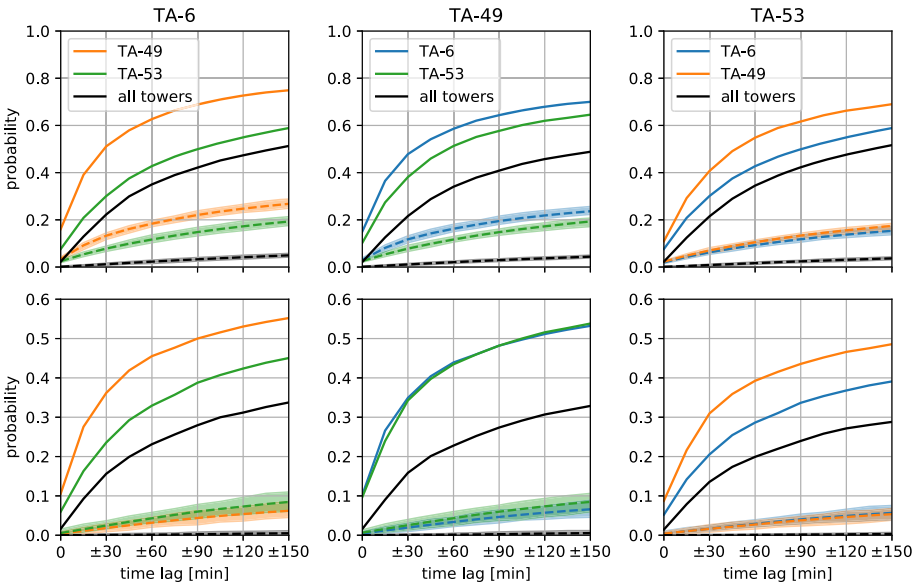

Fig. 9 Probability of contemporaneous wSBL to vSBL (top row) and vSBL to wSBL transitions (bottom row) occurring within a specified time window between the different towers for observational data (solid lines). Dashed lines indicate the mean probabilities of 100 different 25-year theoretical simulations assuming statistically independent regime sequences between the tower sites. The coloured range represents the minimum and maximum values in the different simulations

of initial regime occupation within a night (Table 1), the p.d.f.s of the first transition time in a night (not shown, but similar to Fig. 5, upper panel), and the p.d.f. of event duration (Fig. 5, lower panel). Observed results are then compared to the distribution of these null hypothesis regime sequences. Another approach to generate null hypothesis realizations would be to use the transition probability matrices determined from the HMM analysis in freely-running Markov chains. However, in AHM19 we have demonstrated that freely-running Markov chains cannot adequately reproduce SBL statistics of interest (such as the regime duration distribution).

The probabilities of simultaneous and contemporaneous turbulence collapse events are higher than for contemporaneous turbulence recovery events (Fig. 9). We find that the probability of simultaneous turbulence collapses between pairs of tower sites is between 10 % to 20 %. Probabilities within a $\pm$ 15 minute time window increase to about 40 % between TA-6 and TA-49 and 25 % to 30 % between these towers and TA-53. The probability of contemporaneous transitions levels off at about 60 % to 75 % for time windows of four-hour width. The much larger probabilities of contemporaneous turbulence collapses than would be expected from statistically independent regime sequences (illustrated by dashed lines) demonstrate that, like regime occupation, regime transitions are statistically dependent over the distance of this tower network. Such synchronization is not surprising for the initial turbulence collapse at the nocturnal transition, as surface radiative cooling rates are influenced by large-scale conditions (cf. AM19b). Synchronization of subsequent transitions and of turbulence recovery events is of more interest.

The probability of simultaneous turbulence recovery events between pairs of tower sites ranges between 5 % to 10 %, and the probabilities of contemporaneous transitions level off

at about 50 % as the lag window is increased. The most likely timing of contemporaneous transitions is within a one-hour window centred around the reference transitions, as the most rapid changes of the probabilities with lag are within this time window. These probabilities are also much higher than would be expected from statistically independent simulated regime sequences. Interpreting vSBL to wSBL transitions as often resulting from intermittent turbulence events, our results suggest that such events can either propagate across the tower domain or be of a spatial scale larger than the observational domain. Large-scale processes likely also contribute to synchronized turbulence recoveries. In AM19b, we showed that radiative changes due to changing low-level cloud cover have a stronger connection with regime transitions than other large-scale changes, such as of the geostrophic wind. However, the advection of low-level cloud decks is generally rare in this region (e.g., Rishel et al. 2003; Bruggeman 2017).

Contemporaneous regime transitions across all three stations are less probable than between any pair of towers, but again more likely than would be expected by chance under the null hypothesis of independence (Fig. 9). Simultaneous turbulence collapses occur only about 3 % of the time across the whole tower network domain. However, probabilities within a $\pm$ 2 hour time window increase to about 50 % for turbulence collapse and about 40 % for turbulence recovery events, again with largest increases within a $\pm$ 30 min time window.

Time lag p.d.f.s of contemporaneous turbulence collapse between pairs of towers display symmetric distributions around a narrow peak at zero indicating that wSBL to vSBL transitions are not associated with a preferred propagation direction across the tower domain (not shown). This result is consistent with the dominant role of large-scale influences such as radiative cooling causing turbulence collapse. Whilst simultaneous turbulence recoveries between TA-6 and TA-49 are the most likely, contemporaneous vSBL to wSBL transitions between those sites and TA-53 are skewed towards slightly earlier (15 min, the averaging time of the data) occurrences at TA-53 (not shown). These results suggest a preferred propagation direction of contemporaneous turbulence recovery events uphill from TA-53 to the other two towers.

Joint probability distributions of contemporaneous SBL regime transitions at pairs of towers with a transition at a third site as reference show that transitions of both kinds most likely occur simultaneously between TA-6 and TA-49 and within $\pm$ 30 min between those towers and TA-53 (Fig. 10). The joint probability density distributions further reveal that transitions at TA-6 and TA-49 are relatively well synchronized (as almost none occur outside of $\pm$ 30 minute time window), whereas TA-53 shows a larger variability in the time lags. Relative to TA-6 and TA-49 the wSBL to vSBL transitions are more likely to occur slightly later at TA-53 and turbulence recovery events are more likely to occur earlier. Conditioned on the timing of transitions at TA-53, there is an evident temporal offset of transitions at the other towers. Lag statistics computed from simulated null hypothesis regime sequences do not resemble those of observations.

3.5 State Variable Characteristics for Contemporaneous Transitions

The results above demonstrate that contemporaneous SBL regime transitions are more likely than would be expected from statistically independent regime sequences (particularly for vSBL to wSBL transitions). We now further consider the relationship between contemporaneous transitions and SBL characteristics.

We investigate whether the presence or absence of contemporaneous SBL regime transitions can be associated with the boundary-layer state preceding the transition at individual

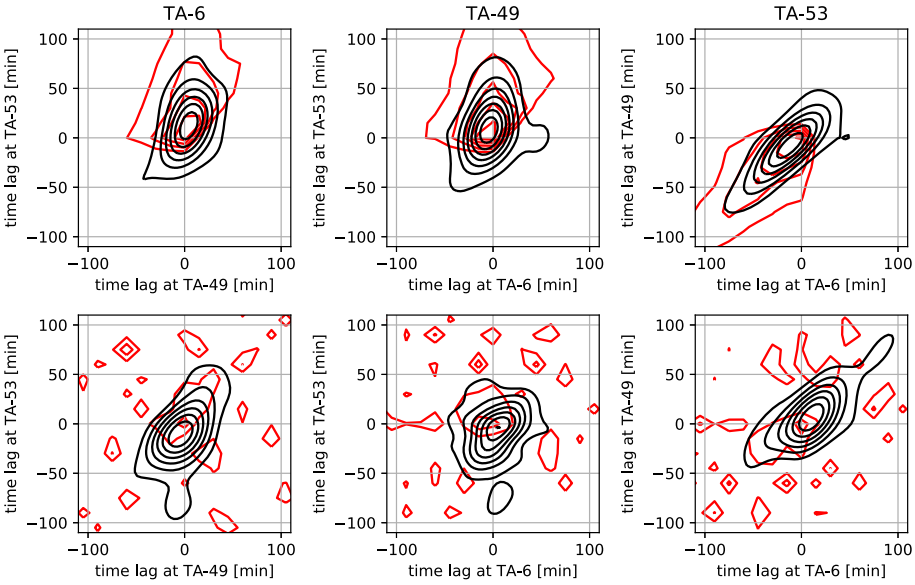

Fig. 10 Joint p.d.f.s of the time lags between the contemporaneous wSBL to vSBL transitions (upper row) and vSBL to wSBL transitions (lower row) occurring across all tower sites (black contours). These joint p.d.f.s are compared to the joint p.d.f.s of 100 different 25-year theoretical simulations assuming statistically independent regime sequences between the tower sites (red lines). The bivariate joint probability density distributions are calculated with the multivariate kernel density estimation of O'Brien et al. (2014, 2016)

reference sites or averaged across the tower network. However, we find that none of wind speed, wind speed shear, stratification, bulk Richardson number (between 46 and 11.5 m), TKE, σ_w, or the tendencies of these quantities, predict either contemporaneous or non-contemporaneous transitions. We draw this conclusion from the fact that p.d.f.s of those variables conditioned on the occurrence of contemporaneous transitions and preceding reference transitions overlap substantially with those obtained for non-contemporaneous transitions (not shown). Furthermore, these quantities at different towers are not correlated in the time preceding contemporaneous transitions (not shown). Consistent with this unpredictability is the fact that no clear association exists between the time lag of contemporaneous transitions and advective propagation time (not shown). Specifically, the advective time scales based on the hourly mean $\|U\|$ around contemporaneous transitions at pairs of sites show no relation with the measured time lags. Contemporaneous turbulence collapse and recovery events are found to be associated with upwind and downwind transition propagation. For turbulence recovery events, this result is consistent with previous observations that the structure and propagation of intermittent turbulence events are only weakly dependent on the mean wind (e.g., Rees and Mobbs 1988; Coulter and Doran 2002; Lang et al. 2018). In summary, there is no evident relationship between the state of the boundary layer and the occurrence or absence of contemporaneous transitions across the tower network.

3.6 A Typology of Contemporaneous Turbulence Recovery Transitions

As discussed above, the spatial dependence of turbulence recovery events suggests that these events are related to synoptic-scale changes or intermittent turbulence events of the scale of,

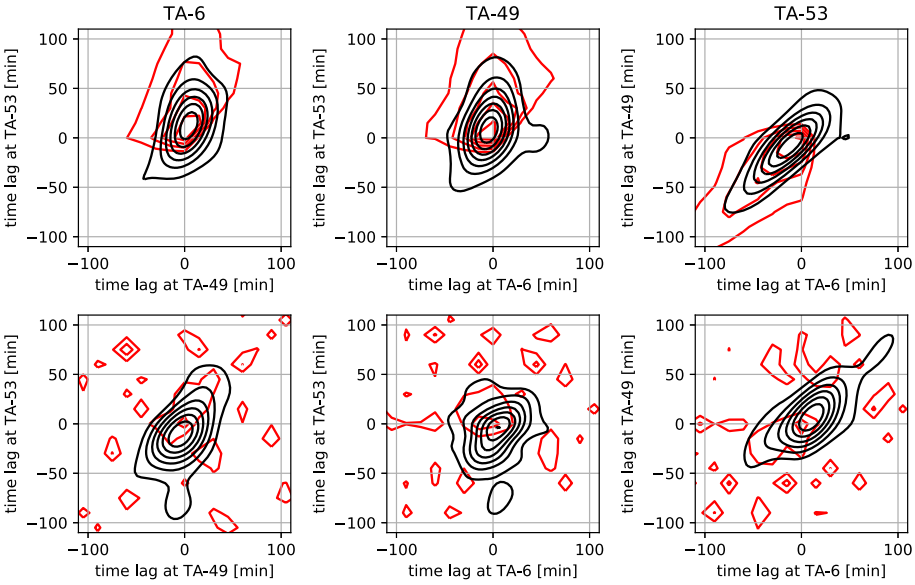

Fig. 11 Four different types of turbulence recovery events occurring contemporaneously at all tower stations (columns;). The evolutions of the fluctuations of the vertical wind component (σ_w; first row), wind speeds (U, second row), potential temperatures (Θ; third row), and stratification ($\Theta_{46} - \Theta_{1.2}$; fourth row) are depicted in the 3 h before and after the vSBL to wSBL transitions with respect to the timing of the transitions at TA-6 (time zero referring to the different dates; LT = UTC – 6 h). The times of the vSBL to wSBL transitions at TA-49 and TA-53 is indicated by vertical dashed lines. Solid and dotted lines illustrate measurements respectively at 46 m and closest to the surface (respectively 11.5 m and 1.2 m for measurements related to wind speeds and temperature). Note that the vertical axes across all plots differ

or propagating through, the tower domain. The relatively low temporal and spatial resolutions of the data used in this study do not allow us to systematically assess these alternatives. However, having inspected σ_w time series in the 6 h around the occurrence of contemporaneous turbulence recovery events, we find that such transitions can be grouped subjectively into four broad types, which are illustrated in Fig. 11. These examples are representative of the types they represent, each of which include many such cases.

The first subjectively determined type of contemporaneous turbulence recovery events (Type I) is associated with initially relatively steady and weak σ_w values followed by a sudden increase in σ_w and wind speed and a rapid breakdown of the stratification (Fig. 11; first column). During Type I events σ_w magnitudes increase by about an order of magnitude, with corresponding changes of all observed variables at all observational levels. After their sudden increase, turbulence intensities decrease relatively rapidly, accompanied by an increase in stratification and a weakening of the winds. Type I events last about 1.5 to 2.5 h, consistent with the maximum in the wSBL event duration p.d.f.s (cf. Fig. 5 and AM19b).

Type II events are characterized by a steady (and relative to Type I slow) increase in σ_w and wind speed (Fig. 11; second column). Shortly after the transition (marked by a rapid breakdown of the stratification), wind speed and σ_w level off at steady values. Such contemporaneous vSBL to wBSL transitions are associated with highly correlated changes of all observed atmospheric variables at all levels across the tower network.

Type III transitions are characterized by a modest increase in σ_w and wind speed for about one to three hours followed by an immediate modest decrease in these variables at a similar

rate (Fig. 11; third column). During such transitions, peaks in the σ_w and wind speed follow the regime transitions. In contrast to Types I and II, in which variables in all levels change in a comparable manner, during Type III events the near surface temperatures are relatively unaffected by the transitions, whereas temperatures aloft tend to increase before the transition and drop rapidly after it. The lowest σ_w values in the vSBL occur just before the transition, at the time that the inversion is strongest due to warming aloft. Subsequent to the transition, the stratification weakens and σ_w increases.

In comparison to the other types, Type IV of contemporaneous vSBL to wSBL transitions is much less organized (Fig. 11; fourth column). Values of σ_w preceding the vSBL to wSBL transitions are generally larger than during the other transitions, consistent with relatively weak stratifications. Consistently, the σ_w values demonstrate weaker changes across the transitions. During this type of contemporaneous transitions, time series of variables across the tower network are rather uncorrelated.

These four types demonstrate distinct features, which we interpret as being associated with different mechanisms driving these contemporaneous transitions. We associate Type I events with the occurrence of an intermittent turbulence event transporting momentum towards the surface and breaking down the vSBL. As these events occur in bursts, the radiative cooling at the surface results in a relatively fast renewal of the inversion and weakening of turbulence intensity. We interpret the steady increases of σ_w and wind speeds in Type II as being caused by gradual synoptic-scale increases in pressure gradient force. Type II events are accompanied by cooling rates that remain relatively constant across the transitions. These characteristics are suggestive of the arrival of a low-pressure system. The fact that Type III events are associated with temperature changes aloft but not at the surface suggests that the transition is driven by advective processes (such that the transition results from a change aloft due to advection from warm air to cooler air). Finally, given the lack of coherent changes across towers, we interpret Type IV events as contemporaneous events that occur simply by chance. This type of contemporaneous transitions is only found for relatively weak inversions with generally larger turbulence intensities preceding the transitions. Such a vSBL configuration might be more vulnerable to smaller, more localized intermittent turbulence events.

The fact that Type I events are not uncommon is particularly interesting, and suggests that high-intensity intermittent turbulence events which exceed the scale of the tower domain or propagate relatively fast are not a rarity in this region. We note again that our typology is subjective and the physical mechanisms invoked are interpretations. Repeating this analysis with more comprehensive datasets (specifically including information about the large-scale environment) would be a valuable test of these interpretations.

4 Conclusions

Data from a network of three towers at the Los Alamos National Laboratory have been analyzed to investigate the spatial dependence of regime occupation and regime transitions in the SBL, based on regime occupation time series from Hidden-Markov-model (HMM) analyses. Regime transitions at these locations are common and occur in about 75 % of all nights.

The regime occupation statistics across the considered tower sites demonstrate that vSBL conditions are more probable than wSBL conditions consistent with the effective radiative cooling and low wind conditions in this region. Our results indicate that winds during wSBL

conditions are likely linked to the large-scale meteorological conditions whereas in the vSBL flow patterns are influenced by local characteristics of the terrain.

Across the network of towers, the regime occupation and regime statistics are found to be spatially-dependent, as joint and conditional probabilities are much larger than would be expected from statistically independent regime occupation sequences. Flows at towers occupy different regimes only for 46-m spatial-mean wind speeds below a threshold of about 7 $\mathrm{m\,s^{-1}}$. Beyond this threshold, only shared wSBL conditions occur. The strong correlation of wind variations across the tower domain indicates that spatial variations in SBL regime occupation are primarily due to local processes.

The joint probability of shared very persistent wSBL nights (without any transitions) is larger than that of very persistent vSBL nights, consistent with the fact that very persistent wSBL nights are caused by strong winds associated with synoptic-scale disturbances. Very persistent vSBL nights, on the other hand, are associated with weak-wind conditions which can easily be perturbed by localized intermittent turbulence events occurring at one rather than at all sites.

The relatively high probability of contemporaneous regime transitions (defined as occurring within a narrow time window across different towers) further demonstrates high spatial dependence of transitions between tower sites. Contemporaneous turbulence collapse events are more frequent than reverse transitions and are most likely to occur simultaneously. While contemporaneous turbulence recovery events are also likely to occur simultaneously, short time lags between the site at the lowest altitude and those at higher elevations are slightly more probable. In general, contemporaneous regime transitions do not have a preferred propagation direction.

While both turbulence collapse and recovery events can be caused by large-scale forcing, the occurrence of turbulence recovery events is more often linked to smaller-scale phenomena such as intermittent turbulence events (e.g., Coulter and Doran 2002; Medeiros and Fitzjarrald 2014). The large probability of contemporaneous recovery events is therefore surprising. Analyses of time series of the turbulence intensity provides evidence of transitions produced by high-intensity intermittent turbulence events which are either of larger scale than the tower network domain, or propagate faster than the time resolution of the measurements can capture. Further investigation of the physical mechanisms driving contemporaneous vSBL to wSBL transitions is an intriguing direction for future research.

The structure of regime dependence clearly suggests that on length scales of about 10 km all regime statistics are spatially dependent in the region of complex terrain being considered. The broad spatial extent of homogenous wSBL conditions for larger wind speeds is consistent with the spatial dependence of strong turbulent fluxes found in Medeiros and Fitzjarrald (2014). Their characterization of the patchiness of turbulent fluxes for vSBL conditions cannot directly be related to our results as the data used here have a coarser time resolution. However, our results suggest that the spatial dependence scale of SBL regime patches under weak-wind conditions can be on length scales larger than the inter-tower distances considered here. We also find that aspects of the spatial dependence below 10 km are not necessarily uniform across the tower domain as the local topographic characteristics at individual towers can affect details of the dependence structure, also consistent with the findings of Medeiros and Fitzjarrald (2015). Taken together, these results suggest that when parametrizing fluxes in the SBL, deterministic long-tailed similarity functions will not suffice for models with horizontal resolutions of several kilometres. If explicitly stochastic representations of SBL regime patches are used (e.g., AHM19), an explicit treatment of dependence between adjacent grid boxes is necessary if the resolution is lower than a few kilometres.

The tower network considered is not of sufficient size to determine the upper limit of spatial dependence of SBL regime statistics. The establishment of more extensive tower networks to address this question is a valuable direction of future research. Another interesting direction of future research could be quantifying in a more systematic way whether regime transitions (in particular vSBL to wSBL transitions) propagate through a network of towers. While our results suggest that on scales of about 10 km contemporaneous turbulence recovery events are sometimes linked to the same intermittent turbulence event, higher resolution data are needed for a more detailed analysis of physical mechanisms. A promising experiment which can be used to address that question is the pilot field campaign in Perdigão, Portugal, conducted in 2017. In this field campaign, observations were taken at a network of over 50 different towers over an area of four square kilometres. Finally, more research has to be conducted across a variety of different conditions (for instance, more homogeneous terrain and different surface types) in order to assess to what degree the spatial regime structures found in this study can be generalized or are specific to this location.

Acknowledgements We would like to thank the team of the Los Alamos National Laboratory (LANL) for making data from the Environmental Monitoring Plan (EMP) freely available under http://environweb.lanl.gov/weathermachine/data_request_green_weather.asp. The Japan Aerospace Exploration Agency (JAXA) is thanked for providing data of topographical elevation from the Advanced Land Observing Satellite (ALOS) Global Digital Surface Model. We would like to thank Amber Holdsworth for helpful discussions. Carsten Abraham and Adam H. Monahan are supported by the Discovery Grant Program of the Natural Sciences and Engineering Research Council Canada (NSERC). The authors would like to thank three anonymous reviewers for helpful comments which improved the manuscript.

References

Abraham C, Monahan AH (2019a) Climatological features of the weakly and very stably stratified nocturnal boundary layers Part I: state variables containing information about regime occupation. J Atoms Sci 76:3455–3484. https://doi.org/10.1175/JAS-D-18-0261.1

Abraham C, Monahan AH (2019b) Climatological features of the weakly and very stably stratified nocturnal boundary layers Part II: regime occupation and transition statistics and the influence of external drivers. J Atmos Sci 76:3485–3504. https://doi.org/10.1175/JAS-D-19-0078.1

Abraham C, Monahan AH (2019c) Climatological features of the weakly and very stably stratified nocturnal boundary layers Part III: the structure of meteorological state variables in persistent regime nights and across regime transitions. J Atmos Sci 76:3505–3527. https://doi.org/10.1175/JAS-D-18-0274.1

Abraham C, Holdsworth AM, Monahan AH (2019) A prototype stochastic parameterization of regime behaviour in the stably stratified atmospheric boundary layer. Nonlinear Process Geophys 26:401–427. https://doi.org/10.5194/npg-26-401-2019

Acevedo OC, Fitzjarrald DR (2003) In the core of the night-effects of intermittent mixing on a horizontally heterogeneous surface. Boundary-Layer Meteorol 106(1):1–33. https://doi.org/10.1023/A:1020824109575

Acevedo OC, Moraes OLL, Degrazia GA, Medeiros LE (2006) Intermittency and the exchange of scalars in the nocturnal surface layer. Boundary-Layer Meteorol 119(1):41–55. https://doi.org/10.1007/s10546-005-9019-3

Acevedo OC, Mahrt L, Puhales FS, Costa FD, Medeiros LE, Degrazia GA (2016) Contrasting structures between the decoupled and coupled states of the stable boundary layer. Q J R Meteorol Soc 142(695):693–702. https://doi.org/10.1002/qj.2693

Acevedo OC, Maroneze R, Costa FD, Puhales FS, Nogueira Martins LG, Soares de Oliveira PE, Mortarini L (2019) The nocturnal boundary layer transition from weakly to very stable. Part 1: observations. Q J R Meteorol Soc. https://doi.org/10.1002/qj.3642

Anfossi D, Oettl D, Degrazia G, Goulart A (2005) An analysis of sonic anemometer observations in low wind speed conditions. Boundary-Layer Meteorol 114(1):179–203. https://doi.org/10.1007/s10546-004-1984-4

Ansorge C, Mellado JP (2014) Global intermittency and collapsing turbulence in the stratified planetary boundary layer. Boundary-Layer Meteorol 153(1):89–116. https://doi.org/10.1007/s10546-014-9941-3

Basu S, Porté-agel F, Foufoula-Georgiou E, Vinuesa JF, Pahlow M (2006) Revisiting the local scaling hypothesis in stably stratified atmospheric boundary-layer turbulence: an integration of field and laboratory measurements with large-eddy simulations. Boundary-Layer Meteorol 119(3):473–500. https://doi.org/10.1007/s10546-005-9036-2

Blumen W, Banta R, Burns SP, Fritts DC, Newsom R, Poulos GS, Sun J (2001) Turbulence statistics of a Kelvin-Helmholtz billow event observed in the night-time boundary layer during the cooperative atmosphere-surface exchange study field program. Dyn Atmos Oceans 34(2–4):189–204. https://doi.org/10.1016/S0377-0265(01)00067-7

Bonin TA, Blumberg WG, Klein PM, Chilson PB (2015) Thermodynamic and turbulence characteristics of the southern Great Plains nocturnal boundary layer under differing turbulent regimes. Boundary-Layer Meteorol 157(3):401–420. https://doi.org/10.1007/s10546-015-0072-2

Bruggeman DA (2017) Los Alamos climatology 2016 update. Los Alamos National Laboratory. https://permalink.lanl.gov/object/tr?what=info:lanl-repo/lareport/LA-UR-17-21060, Tech rep. Accessed 12 Nov 2019

Coulter RL, Doran JC (2002) Spatial and temporal occurrences of intermittent turbulence during CASES-99. Boundary-Layer Meteorol 105(2):329–349. https://doi.org/10.1023/A:1019993703820

Donda JMM, van Hooijdonk IGS, Moene AF, Jonker HJJ, van Heijst GJF, Clercx HJH, van de Wiel BJH (2015) Collapse of turbulence in stably stratified channel flow: a transient phenomenon. Q J R Meteorol Soc 141(691):2137–2147. https://doi.org/10.1002/qj.2511

Doran JC (2004) Characteristics of intermittent turbulent temperature fluxes in stable conditions. Boundary-Layer Meteorol 112(2):241–255. https://doi.org/10.1023/B:BOUN.0000027907.06649.d0

Flores O, Riley JJ (2011) Analysis of turbulence collapse in the stably stratified surface layer using direct numerical simulation. Boundary-Layer Meteorol 139(2):241–259. https://doi.org/10.1007/s10546-011-9588-2

Goulart AGO, Degrazia GA, Acevedo OC, Anfossi D (2007) Theoretical considerations of meandering winds in simplified conditions. Boundary-Layer Meteorol 125(2):279–287. https://doi.org/10.1007/s10546-007-9179-4

He Y, McFarlane NA, Monahan AH (2012) The influence of boundary layer processes on the diurnal variation of the climatological near-surface wind speed probability distribution over land. J Clim 115(D04):103. https://doi.org/10.1175/JCLI-D-11-00321.1

Holdsworth AM, Monahan AH (2019) Turbulent collapse and recovery in the stable boundary layer using an idealized model of pressure-driven flow with a surface energy budget. J Atmos Sci 76(5):1307–1327. https://doi.org/10.1175/JAS-D-18-0312.1 (Submitted to)

Holdsworth AM, Rees T, Monahan AH (2016) Parameterization sensitivity and instability characteristics of the maximum sustainable heat flux framework for predicting turbulent collapse. J Atmos Sci 73:3527–3540. https://doi.org/10.1175/JAS-D-16-0057.1

Lang F, Belušić D, Siems S (2018) Observations of wind-direction variability in the nocturnal boundary layer. Boundary-Layer Meteorol 166(1):51–68. https://doi.org/10.1007/s10546-017-0296-4

Mahrt L (1998) Nocturnal boundary-layer regimes. Boundary-Layer Meteorol 88(2):255–278. https://doi.org/10.1023/A:1001171313493

Mahrt L (2010) Common microfronts and other solitary events in the nocturnal boundary layer. Q J R Meteorol Soc 136(652):1712–1722. https://doi.org/10.1002/qj.694

Mahrt L (2011) The near-calm stable boundary layer. Boundary-Layer Meteorol 140(3):343–360. https://doi.org/10.1007/s10546-011-9616-2

Mahrt L (2014) Stably stratified atmospheric boundary layers. Annu Rev Fluid Mech 46:23–45. https://doi.org/10.1146/annurev-fluid-010313-141354

Mahrt L, Thomas C, Richardson S, Seaman N, Stauffer D, Zeeman M (2013) Non-stationary generation of weak turbulence for very stable and weak-wind conditions. Boundary-Layer Meteorol 147(2):179–199. https://doi.org/10.1007/s10546-012-9782-x

Mahrt L, Sun J, Stauffer D (2015) Dependence of turbulent velocities on wind speed and stratification. Boundary-Layer Meteorol 155(1):55–71. https://doi.org/10.1007/s10546-014-9992-5

Mauritsen T, Svensson G (2007) Observations of stably stratified shear-driven atmospheric turbulence at low and high Richardson numbers. J Atmos Sci 64:645–655. https://doi.org/10.1175/JAS3856.1

McCabe A, Brown AR (2007) The role of surface heterogeneity in modelling the stable boundary layer. Boundary-Layer Meteorol 122(3):517–534. https://doi.org/10.1007/s10546-006-9119-8

Medeiros LE, Fitzjarrald DR (2014) Stable boundary layer in complex terrain. Part I: linking fluxes and intermittency to an average stability index. J Appl Meteorol Clim 53:2196–2215. https://doi.org/10.1175/JAMC-D-13-0345.1

Medeiros LE, Fitzjarrald DR (2015) Stable boundary layer in complex terrain. Part II: geometrical and sheltering effects on mixing. J Appl Meteorol Clim 54(1):170–188. https://doi.org/10.1175/JAMC-D-13-0346.1

Monahan AH, Rees T, He Y, McFarlane N (2015) Multiple regimes of wind, stratification, and turbulence in the stable boundary layer. J Atmos Sci 72:3178–3198. https://doi.org/10.1175/JAS-D-14-0311.1

Mortarini L, Maldaner S, Moor LP, Stefanello MB, Acevedo O, Degrazia G, Anfossi D (2016) Temperature auto-correlation and spectra functions in low-wind meandering conditions. Q J R Meteorol Soc 142(698):1881–1889. https://doi.org/10.1002/qj.2796

Mortarini L, Cava D, Giostra U, Costa FD, Degrazia G, Anfossi D, Acevedo O (2019) Horizontal meandering as a distinctive feature of the stable boundary layer. J Atmos Sci 76(10):3029–3046. https://doi.org/10.1175/JAS-D-18-0280.1

Nappo CJ (1991) Sporadic breakdowns of stability in the PBL over simple and complex terrain. Boundary-Layer Meteorol 54(1):69–87. https://doi.org/10.1007/BF00119413

Nappo C, Sun J, Mahrt L, Belušić D (2014) Determining wave-turbulence interactions in the stable boundary layer. Bull Am Meteorol Soc 95:ES11–ES13. https://doi.org/10.1175/BAMS-D-12-00235.1

Newsom RK, Banta RM (2003) Shear-flow instability in the stable nocturnal boundary layer as observed by Doppler Lidar during CASES-99. J Atmos Sci 60:16–33. https://doi.org/10.1175/1520-0469(2003)060<0016:SFIITS>2.0.CO;2

O'Brien TA, DCollins W, ARauscher S, Ringler TD (2014) Reducing the computational cost of the ECF using a nuFFT: a fast and objective probability density estimation method. Comput Stat Data Anal 79:222–234. https://doi.org/10.1016/j.csda.2014.06.002

O'Brien TA, Kashinath K, Cavanaugh NR, DCollins W, O'Brien JP (2016) A fast and objective multidimensional kernel density estimation method: fastKDE. Comput Stat Data Anal 101:148–160. https://doi.org/10.1016/j.csda.2016.02.014

Rabiner LR (1989) A tutorial on hidden Markov models and selected applications in speech recognition. Proc IEEEE 77:257–286. https://doi.org/10.1109/5.18626

Rees JM, Mobbs SD (1988) Studies of internal gravity waves at Halley Base, Antarctica, using wind observations. Q J R Meteorol Soc 114(482):939–966. https://doi.org/10.1002/qj.49711448206

Rishel J, Johnson S, Holt D (2003) Meteorological monitoring at Los Alamos. Los Alamos National Progress Report LA-UR-03-9097. Los Alamos National Laboratory. https://envweb.lanl.gov/weathermachine/downloads/LA-UR-03-8097_webcopy.pdf, Tech rep. Accessed 12 Nov 2019

Sun J, Burns SP, Lenschow DH, Banta R, Newsom R, Coulter R, Frasier S, Ince T, Nappo C, Cuxart J, Blumen W, Lee X, Hu XZ (2002) Intermittent turbulence associated with a density current passage in the stable boundary layer. Boundary-Layer Meteorol 105(2):199–219. https://doi.org/10.1023/A:1019969131774

Sun J, Lenschow DH, Burns SP, Banta RM, Newsom RK, Coulter R, Frasier S, Ince T, Nappo C, Balsley BB, Jensen M, Mahrt L, Miller D, Skelly B (2004) Atmospheric disturbances that generate intermittent turbulence in nocturnal boundary layers. Boundary-Layer Meteorol 110(2):255–279. https://doi.org/10.1023/A:1026097926169

Sun J, Mahrt L, Banta RM, Pichugina YL (2012) Turbulence regimes and turbulence intermittency in the stable boundary layer during CASES-99. J Atmos Sci 69:338–351. https://doi.org/10.1175/JAS-D-11-082.1

Sun J, Mahrt L, Nappo C, Lenschow DH (2015a) Wind and temperature oscillations generated by wave-turbulence interactions in the stably stratified boundary layer. J Atmos Sci 72:1484–1503. https://doi.org/10.1175/JAS-D-14-0129.1

Sun J, Nappo CJ, Mahrt L, Belušić D, Grisogono B, Stauffer DR, Pulido M, Staquet C, Jiang Q, Pouquet A, Yagüe C, Galperin B, Smith RB, Finnigan JJ, Mayor SD, Svensson G, Grachev AA, Neff WD (2015b) Review of wave-turbulence interactions in the stable atmospheric boundary layer. Rev Geophys 53(3):956–993. https://doi.org/10.1002/2015RG000487

Sun J, Lenschow DH, LeMone MA, Mahrt L (2016) The role of large-coherent-eddy transport in the atmospheric surface layer based on CASES-99 observations. Boundary-Layer Meteorol 160(1):83–111. https://doi.org/10.1007/s10546-016-0134-0

van de Wiel BJH, Moene AF, Steeneveld GJ, Hartogensis OK, Holtslag AAM (2007) Predicting the collapse of turbulence in stably stratified boundary layers. Flow Turbul Combust 79(3):251–274. https://doi.org/10.1007/s10494-007-9094-2

van de Wiel BJH, Vignon E, Baas P, van Hooijdonk IGS, van der Linden SJA, van Hooft JA, Bosveld FC, de Roode SR, Moene AF, Genthonc C (2017) Regime transitions in near-surface temperature inversions: a conceptual model. J Atmos Sci 74:1057–1073. https://doi.org/10.1175/JAS-D-16-0180.1

van Hooijdonk IGS, Donda JMM, Bosveld HJHCFC, van de Wiel BJH (2015) Shear capacity as prognostic for nocturnal boundary layer regimes. J Atmos Sci 72:1518–1532. https://doi.org/10.1175/JAS-D-14-0140.1

van Hooijdonk I, Moene A, Scheffer M, Clercx H, van de Wiel B (2017) Early warning signals for regime transition in the stable boundary layer: a model study. Boundary-Layer Meteorol 162(2):283–306. https://doi.org/10.1007/s10546-016-0199-9

van der Linden S (2020) From Dutch short-lived to Antarctic long-lived stable boundary layers. Ph.D. thesis, Delft University of Technology. https://doi.org/10.4233/uuid:02eef221-2d22-4492-babd-8f8d3f782f8b

Vercauteren N, Klein R (2015) A clustering method to characterize intermittent bursts of turbulence and interaction with submesomotions in the stable boundary layer. J Atmos Sci 72:1504–1517. https://doi.org/10.1175/JAS-D-14-0115.1

Vignon E, van de Wiel BJH, van Hooijdonk IGS, Genthon C, van der Linden SJA, van Hooft JA, Baas P, Maurel W, Traullé O, Casasanta G (2017) Stable boundary-layer regimes at Dome C, Antarctica: observation and analysis. Q J R Meteorol Soc 143(704):1241–1253. https://doi.org/10.1002/qj.2998

Williams AG, Chambers S, Griffiths A (2013) Bulk mixing and decoupling of the nocturnal stable boundary layer characterized using a ubiquitous natural tracer. Boundary-Layer Meteorol 149(3):381–402. https://doi.org/10.1007/s10546-013-9849-3

Zilitinkevich SS, Elperin T, Kleeorin N, Rogachevskii I, Esau I, Mauritsen T, Miles MW (2008) Turbulence energetics in stably stratified geophysical flows: strong and weak mixing regimes. Q J R Meteorol Soc 134(633):793–799. https://doi.org/10.1002/qj.264